

Document downloaded from:

<http://hdl.handle.net/10251/63972>

This paper must be cited as:

Desantes Fernández, JM.; Hoyas Calvo, S.; Gil Megías, A.; Khuong, AD.; Ravet, F. (2014). A RECENT EULERIAN LAGRANGIAN CFD METHODOLOGY FOR MODELING DIRECT INJECTION DIESEL SPRAYS. *International Journal of Computational Methods*. 11(3):1343012-1343029. doi:10.1142/S0219876213430123.



The final publication is available at

<http://dx.doi.org/10.1142/S0219876213430123>

Copyright World Scientific Publishing

Additional Information

# A RECENT EULERIAN-LAGRANGIAN CFD METHODOLOGY FOR MODELLING DIRECT INJECTION DIESEL SPRAYS

**José M. Desantes<sup>1</sup>, Sergio Hoyas<sup>1</sup>, Antonio Gil<sup>1</sup>, Dung Khuong-Anh<sup>1</sup>, and Frédéric Ravet<sup>2</sup>**

<sup>1</sup> CMT-Motores Térmicos, Universitat Politècnica de València  
Valencia 46022, Spain

E-mail: jmdesant@mot.upv.es, serhocal@mot.upv.es, angime@mot.upv.es and ankh2@mot.upv.es

<sup>2</sup> Renault

1 Avenue du Golf 78288, Guyancourt, France

E-mail: frederic.ravet@renault.com

## ABSTRACT

The global objective of this work is to show the capabilities of the Eulerian-Lagrangian Spray Atomization (ELSA) model for the simulation of Diesel sprays in cold starting conditions. Our main topic is to focus in the analysis of spray formation and its evolution at low temperature 255K (-18°C) and non-evaporative conditions. Spray behaviour and several macroscopic properties, included the liquid spray penetration, and cone angle are also characterized. This study has been carried out using different ambient temperature and chamber pressure conditions. Additionally, the variations of several technical quantities, as the area coefficient and effective diameter are also studied. The results are compared with the latest experimental results in this field obtained in our institute. In the meantime, we also compare with the normal ambient temperature at 298 K (25°C) where the numerical validation of the model has shown a good agreement.

**Key words:** *CFD, ELSA, Eulerian, Lagrangian, diesel spray, non-evaporating, atomization.*

## 1. INTRODUCTION

Efficiency standards, emission control and fuel economy have been and are nowadays an immense challenge in the automotive industry. Even though automotive world have made big advances during the last decades in the efficiency of both the gasoline and diesel engines, there are many processes and mechanism that should be improved. These include the necessity of a better understanding of the noise generation, the physics of turbulent flows, combustion processes and contaminant formation and transport. In the field of numerical simulation, Computational Fluid Dynamics (CFD) has established its roles in the car industry to take advantage of it relatively easy implementation, low time consuming and lower cost investment.

The understanding of spray and atomization of diesel spray in the internal combustion engine is very difficult in either experimental or theoretical studies. Fuel spray occurs in a small chamber inside the combustion engine. The fuel comes from a tiny nozzle cross section (hundred micrometers) at very high pressure and everything happens at an extremely short time (few milliseconds). Regardless the reactive part of the processes, diesel spray study includes several fundamentals, and not totally resolved topics, as can be the spray structure itself, break-up and atomization processes, or the behaviour of two-phase turbulent flows.

As Direct Numerical Simulation (DNS) are impossible in the daily product design, due to its immense computational cost, Large Eddy Simulation (LES) model has been applied gradually in studying specific problems in engine simulation together with the continuously increasing powerful computer technology. LES schemes, however, need still a further theoretical development, due to their problems close to walls and that the grid resolution must be adjusted correctly with each particular flow problem and boundary conditions. Thus, the Reynolds-averaged Navier–Stokes (RANS) turbulence models are still the most used methods modelling turbulence due to its relatively good accuracy at a very low computational cost.

RANS approaches in spray modelling using both Eulerian and Lagrangian descriptions are being used in industry for decades. However, each of them has both advantages and disadvantages in modelling the various regions of spray consisting of the dense zone and the downstream dilute zone. Typically the Eulerian description presents better results in the first part of the spray, whereas Lagrangian description is the most widely used in the diluted zone. In the framework of this numerical research, we have used a coupled method for spray and atomization simulation: ELSA model. The original idea was ignited by Vallet et al. in 2001 [1], Blokkeel et al. added an overview in 3D [2], Beau formed many source terms and simulation in his thesis [3], and so on. This algorithm is able to describe the primary break-up and the secondary atomization of the spray, and switches automatically from one description to the other.

This algorithm has been implemented in CD-Adapco Star-CD CFD code conducted together with Renault S.A. The code has been validated previously, showing an excellent agreement with experimental data ([4],[5], and [6]). As it has been said before, in this article, we restrict ourselves to simulate using ELSA methodology in cold conditions.

## 2. COMPUTATIONAL METHOD

As mentioned previously, the ELSA model was first initiated in an article of Vallet et al., 2001 [1]. Several other continuous works, including Beau, 2006 [7], and Ning et al. [8] and so forth also additionally contributed this set of equations. A detail description of governing equations and methodology were presented in Hoyas et al., 2011 ([5] and [6]), and Desportes et al., 2010 ([9], and [10]). In this subsection, the main equations are summarized hereafter in shake of completeness of the paper and a logical explanation of the ELSA model. These equations covered the several regions of the ELSA model, changing from one to another, from now on and in all the regions, the subscript  $l$  stands for liquid and  $g$  stands for gas, whereas  $i, j$  are the direction in space.

### 2.1. Eulerian mixture zone

We define the mean liquid mass fraction,  $\tilde{Y}_l$  as

$$\tilde{Y}_l = \frac{\overline{\rho Y_l}}{\bar{\rho}}, \quad (1)$$

where  $\rho$  is the density and  $Y_l$  is the liquid mass fraction. Intuitively, mean density,  $\bar{\rho}$  is defined as

$$\bar{\rho} = \rho_l \bar{Y}_l + \rho_g (1 - \bar{Y}_l), \quad (2)$$

which is expressed in terms of  $\tilde{Y}_l$  as

$$\frac{1}{\bar{\rho}} = \frac{\tilde{Y}_l}{\rho_l} + \frac{1-\tilde{Y}_l}{\rho_g} \quad (3)$$

Favre averaged mean velocity is defined as

$$\tilde{U}_i = \tilde{Y}_l U_{l,i} + (1-\tilde{Y}_l) U_{g,i} \quad (4)$$

## 2.2. Liquid/gas interface density

A transport equation for liquid surface density,  $\tilde{\Omega}$ , is postulated by analogy with the flame surface density.

$$\frac{\partial \bar{\rho} \tilde{\Omega}}{\partial t} + \frac{\partial \bar{\rho} \tilde{\Omega} \tilde{U}_j}{\partial x_j} = \frac{\partial}{\partial x_j} \left( \bar{\rho} \frac{v_t}{Sc_t} \frac{\partial \tilde{\Omega}}{\partial x_j} \right) + \bar{\rho} \cdot \left( \tilde{\Omega}_{init} + \tilde{\Omega}_{mean} + \tilde{\Omega}_{turb} + \tilde{\Omega}_{coll} + \tilde{\Omega}_{coal} \right) + S_{EL}^{\tilde{\Omega}} \quad (5)$$

Where  $\tilde{\Omega}_{init}$ ,  $\tilde{\Omega}_{mean}$ ,  $\tilde{\Omega}_{turb}$ ,  $\tilde{\Omega}_{coll}$  and  $\tilde{\Omega}_{coal}$  are the initial, mean, turbulence, collision and coalescence value of liquid/gas surface density respectively;  $S_{EL}^{\tilde{\Omega}}$  is the source term of the liquid/gas interface. Beau, 2006 [7] introduced other notion of liquid/gas interface per unity of mass that is defined as  $\tilde{\Omega} = \tilde{\Sigma} / \bar{\rho}$  (m<sup>2</sup>/kg).

## 2.3. Transition zone

We rely on a critical value of the Eulerian liquid volume fraction to decide whether it should turn from Eulerian to Lagrangian formulation (Beau, 2006 [7]). The Lagrangian droplets are formed where spray is assumed to be diluted enough. It follows the below relationship.

$$\tilde{\Phi}_l = \tilde{Y}_l \frac{\bar{\rho}}{\rho_l} \leq \tilde{\Phi}_l^{crit} \quad (6)$$

with  $\tilde{\Phi}_l^{crit}$  stands for the critical value of the Eulerian liquid volume fraction.

The transitional criterion is based on the value of liquid volume fraction that is linked to the ratio of mean free path between two droplets and mean equivalent radius of the droplets in the cell. In our calculation, the transition is done when the liquid volume fraction becomes lower than 0.01 [9]. The transition zone is composed of the computational cells that form the border with the dense zone (i.e. zone where the liquid volume fraction is greater than 0.01) and only one parcel is generated per transition cell and per time step.

The velocity of the droplets is defined as

$$\bar{U}_{l,i} = \tilde{U}_i + \frac{\overline{\rho u_i'' y''}}{\bar{\rho} \tilde{Y}_l} \quad (7)$$

### 3. EXPERIMENTAL DATA AND SETUP

The experimental results used in this paper were conducted in a test rig used to investigate the influence of diesel spray under cold starting conditions [11], installed at CMT Motores Térmicos Institute. This set of experiments, were intended only for studying the macroscopic characteristics of the diesel spray.

#### 3.1. Nozzle geometry and liquid fuel

For this study, a conical nozzle,  $D = 112 \mu\text{m}$  was used. Macián et al., 2003 [12] developed the silicone methodology to determine the internal geometry of the injector as shown in Figure 1. Its main parameters are depicted in Table I.

Table I: Nozzle parameters

Nozzle	r	$D_e$ (inlet diameter)	$D_0$ (out diameter at the nozzle exit)	k-factor
	[ $\mu\text{m}$ ]	[ $\mu\text{m}$ ]	[ $\mu\text{m}$ ]	[-]
N1	42	140	112	2.8

Where the k-factor, a measure of the conicity, is calculated based on the following formula:

$$k - factor = \frac{D_e - D_0}{10} \quad (8)$$

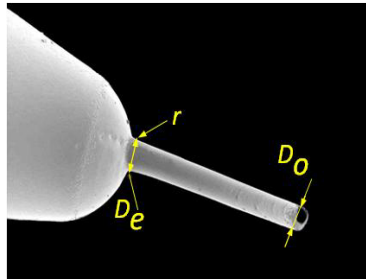


Figure 1: Nozzle geometry and the definition of some basic parameter.

Nitrogen was used to fill the pressurised vessel. ARCTIQUE fuel (ARCT from now on), was investigated. These results were used in order to validate the simulation, and once trusted, another fuel, ELITE – Repsol (REF) has been used. The properties of those fuels are tabulated in Table II.

Table II: Fuel Properties

Fuel type	Liquid Density	Kinematic Viscosity	Dynamic Viscosity	Surface Tension
	( $\text{kg}/\text{m}^3$ )	( $\text{mm}^2/\text{s}$ )	( $\text{kg}/\text{ms}$ )	( $\text{N}/\text{m}$ )
ARCTIQUE (ARCT)	825	2.34	0.00193050	0.0205
ELITE – Repsol (REF)	812	2.06	0.00167272	0.022

### 3.2. Measurement of the injection rate

Bosch, 1966 [13] developed the test rig using Injection Rate Discharge Curve Indicator (IRDCI) to measure the mass flow rate based on the Bosch method. The mass flow rate test rig operates relied on the principle the pressure wave propagation in the liquid column. The pressure wave created a pressure variation, these quantities is then recorded by a piezoelectric sensor located near the nozzle tip.

Using Allievi equation ([14], and [15]) for a simple pressure wave in a steady flows, the pressure increment with respect to the steady pressure,  $\Delta P_m$  is linearly proportional to the liquid flow velocity:

$$\Delta P_m = a \rho_l u \quad (9)$$

Where  $a$  stands for the fuel speed of sound,  $u$  stands for the liquid fuel velocity.

Finally, the injection rate,  $\dot{m}$  is obtained using the following eq.:

$$\dot{m}(t) = \frac{A_{tub} \Delta P_m}{a} \quad (10)$$

where  $A_{tub}$  is the cross section area of the tube.

## 4. BOUNDARY CONDITIONS AND GEOMETRY

In previous articles, a detailed study of the number of cells in the nozzle diameter, axial, radial cells, successive ratio of mesh edges, etc., were performed ([4], [5], and [6]). Hence, the mesh dependency is not taken into account in this study. Similar scales and ratios obtained from these previous works have been applied to build the grid for this nozzle.

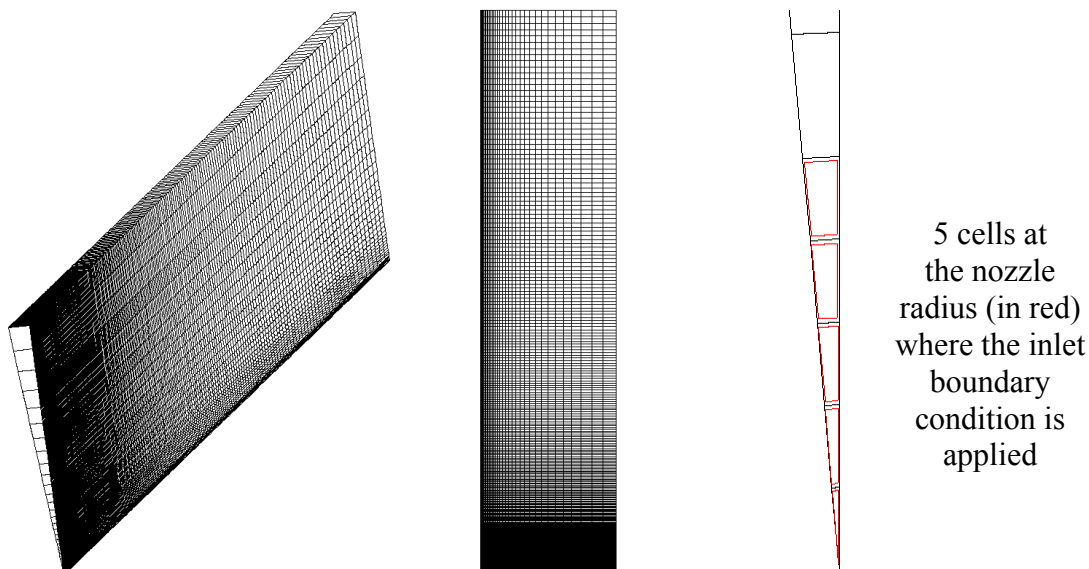


Figure 2: (from the left to the right) An isometric view of the whole computational domain, an aside view and a zoom of front view at nozzle cross section.

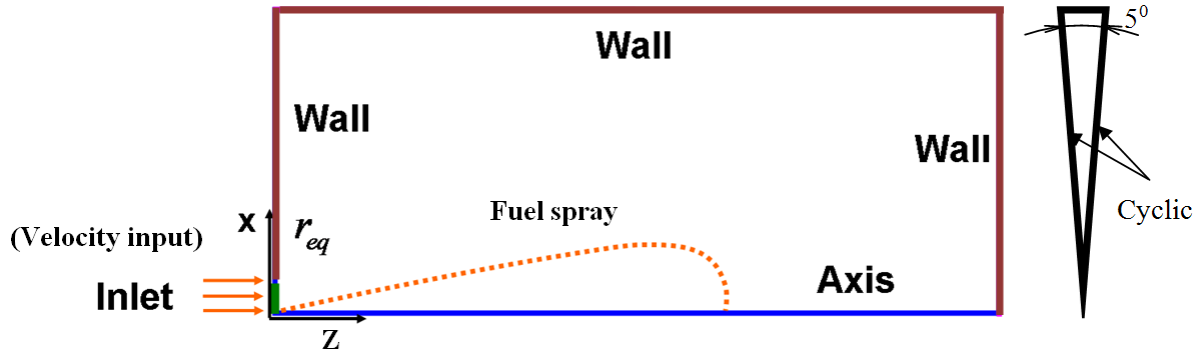


Figure 3: Geometry (front view and side view) & Boundary Conditions.

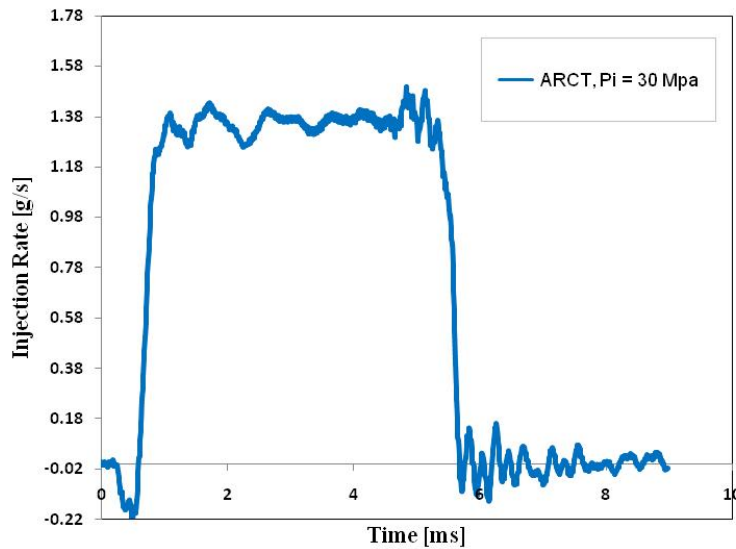


Figure 4: The injection rate of ARCT fuel at  $P_{inj} = 30$  MPa, the ambient temperature  $T = 255$  K, and ambient pressure 2.1 MPa.

The computational domain is a wedge of area  $12 \times 80 \text{ cm}^2$  and an angle of  $5^\circ$  which contains 40,581 vertices and 20,000 cells, plotted in Figure 2. The mesh structure is built in such a way that the smallest cells are in the spray region (where gradients are high) and grows continuously until the end of the grid domain.

Figure 2 and Figure 3 show all boundary conditions for the computational domain. The input velocity at the nozzle exit is calculated directly from the real mass flow rate (injection rate). The velocity radial profile is constant spatially, and an effective diameter has been used instead of real diameter ( $D = 112 \mu\text{m}$ ). This detail is explained more carefully later. The injection rate was measured by León [11] using current available test rig at CMT Motores Térmicos Institute. This injection rate is plotted in Figure 4, corresponding to an injection pressure  $P_{inj} = 30$  MPa, and an injection temperature equal to 293 K.

## 5. RESULTS AND DISCUSSION

In this present section, numerical results are presented and several comparisons with all the measured data are made. For the sake of identically validated results, a spray tip penetration figure and axial velocity along the axis is plotted for all cases hereafter.

As far as the spray tip penetration  $S(t)$  is concerned, the theoretical spray tip penetration applied the Buckingham  $\pi$  theorem [16] is formulated as:

$$S(t) = k \cdot \rho_g^{-0.25} \cdot M_0^{-0.25} \cdot t^{0.5} \cdot \tan^{-0.5} \left( \frac{\theta}{2} \right) \quad (11)$$

Where  $M_0$  is theoretical spray momentum flux,  $k$  adjustment constant is obtained from experimental test,  $t$  at the specific time,  $\theta/2$  is the experimental semi-cone angle. The different injected fuel are examined using the same effective diameter equal to  $100 \mu\text{m}$ , nitrogen ambient pressure with the vessel temperature equal to  $255 \text{ K}$  and the vessel pressure equal to  $2.1 \text{ MPa}$ . Using the same injection rate, there is very little change in the input velocity due to the different liquid fuel density between those fuels, as a result, there are a slightly discrepancy one moving from REF and ARCT at the beginning as shown in Figure 5, but this small variation were sooner eliminated in the vessel conditions at further distance from nozzle exit since the chamber conditions remained the same in both cases.

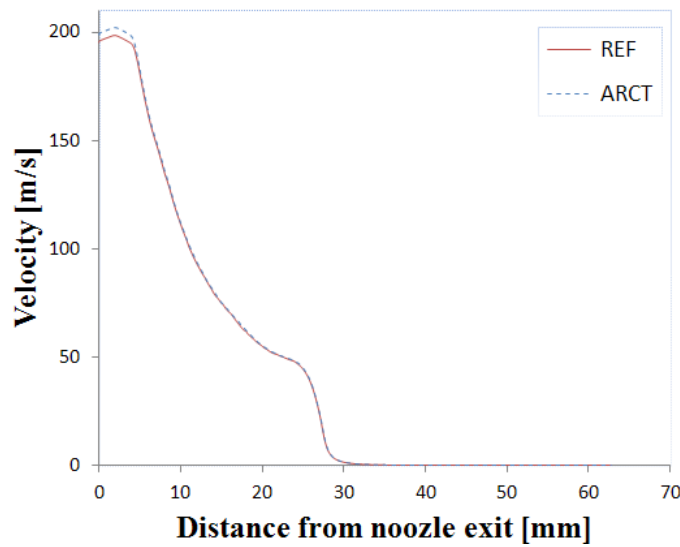


Figure 5: The axial velocity profiles of two type of fuels at the same ambient temperature  $T = 255 \text{ K}$ , and ambient pressure  $2.1 \text{ MPa}$ .

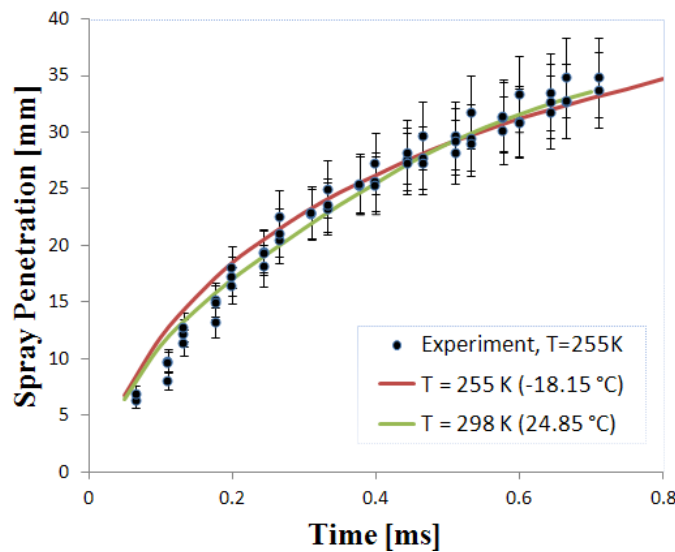


Figure 6: The comparison of the spray tip penetration at the gas ambient temperature of  $255 \text{ K}$ ,  $298 \text{ K}$  and  $P_{\text{amb}} = 2.1 \text{ MPa}$ ,  $P_{\text{amb}} = 2.4 \text{ MPa}$  respectively, and  $P_{\text{inj}} = 30 \text{ MPa}$ . The experiment is shown only for the low ambient temperature at  $255 \text{ K}$ .

As can be seen in Figure 6, a very good agreement between the experimental data and the simulation results in term of spray tip penetration is observed in the plot. For the normal operating temperature ( $\sim 25\text{ }^\circ\text{C}$ ), the model showed extremely fit with the experiment results, there is a very slightly different for the lower vessel temperature levels ( $-18\text{ }^\circ\text{C}$ ), however, it is very small and can be considered the very good prediction of the experimental trend.

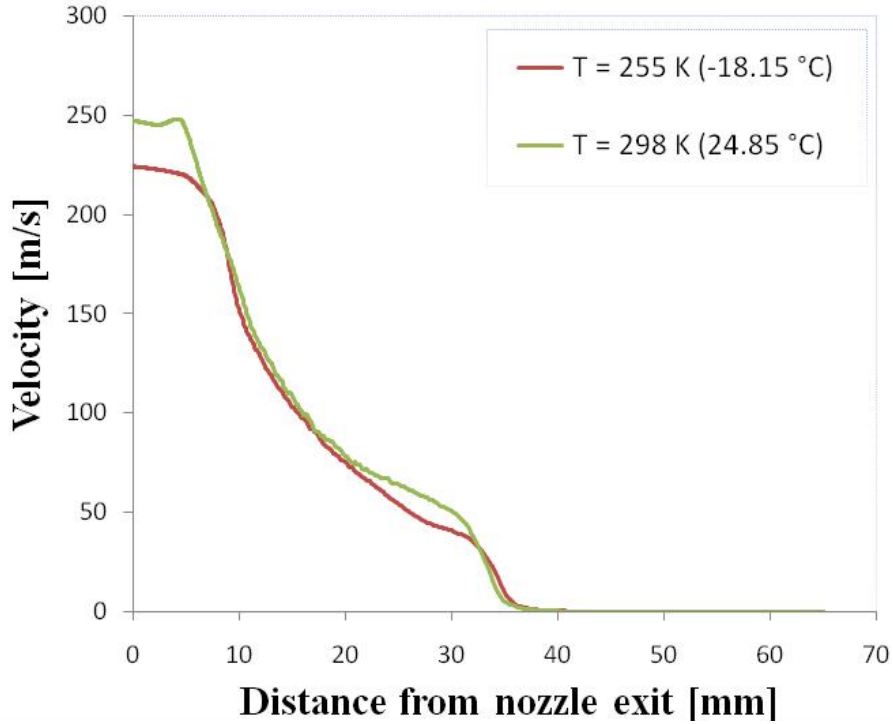


Figure 7: The comparison of the velocity along the axial axis at the gas ambient temperature of 255 K, 298 K and  $P_{amb} = 2.1\text{ MPa}$ ,  $P_{amb} = 2.4\text{ MPa}$  respectively, and  $P_{inj} = 30\text{ MPa}$ .

The comparison of the velocity profile along the axial axis where the set of highest value of velocity are produced was made. In Figure 7, the velocity in the spray axis is recorded. Obviously, for the low ambient temperature, we obtained a lower velocity during the whole injection process, on the other hand, the normal temperature produced a higher axial velocity profile. In the theoretical approach, the velocity along the axis can be calculated using the following equation:

$$U_{axis}(x) = \frac{\dot{M}_0^{1/2}}{\rho_{amb}^{1/2} \left(\frac{\pi}{2\omega}\right)^{1/2} x \tan \frac{\theta}{2}} \quad (12)$$

Where  $\omega$  is the shape factor of the Gaussian distribution, it is equal to 4.6 referred to [17].

As already mentioned in the previous part, since we used the convergent orifice, there is almost no or very less cavitation in the internal nozzle flow. Thus the area coefficient  $C_a$  is approach to 1, to take into account a small effect of the area coefficient equal to 0.98 are used. Eqs. 13 - 15 depicted the relation of  $C_a$  and cross-sectional area, diameter of the desired nozzle.

$$C_a = \frac{A_{eff}}{A_0} \quad (13)$$

With

$$A = \pi \cdot r^2 \quad (14)$$

Where  $A_0$  is the real nozzle exit diameter.

$$C_a = \frac{D_{eff}^2}{D_0^2} \quad (15)$$

With a fixed geometry convergent nozzle, when the area coefficient is moved toward 1, the effective diameter also increased accordingly as seen in Table III.

Table III: Area coefficient and effective diameter

$D_0$ (nozzle exit diameter)	$C_a$ (area coefficient)	$D_{eff}$ (effective diameter)
[ $\mu\text{m}$ ]	[-]	[ $\mu\text{m}$ ]
112	0.98	111
112	0.9	106
112	0.8	100

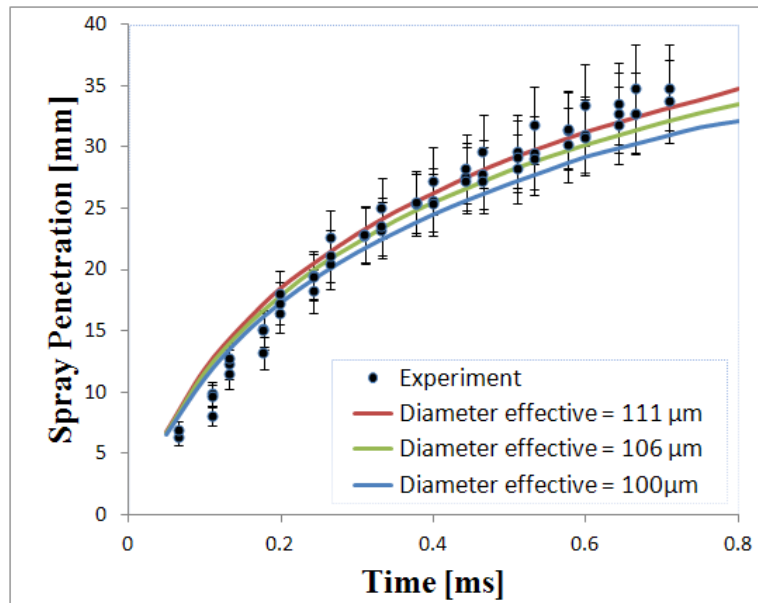


Figure 8: The effect of different effective diameter at 100 $\mu\text{m}$ , 106  $\mu\text{m}$ , and 111 $\mu\text{m}$  on the spray tip penetration at the gas ambient temperature of 255 K.

The macroscopic parameter again is investigated in Figure 8 to study the characterization of the spray, that is the spray penetration. In this figure the higher effective diameter gave the better commitment with the effective diameter equal to 111  $\mu\text{m}$ , for the lower effective diameter, the results are a bit underestimate. It is understandable as the conical nozzle has been used.

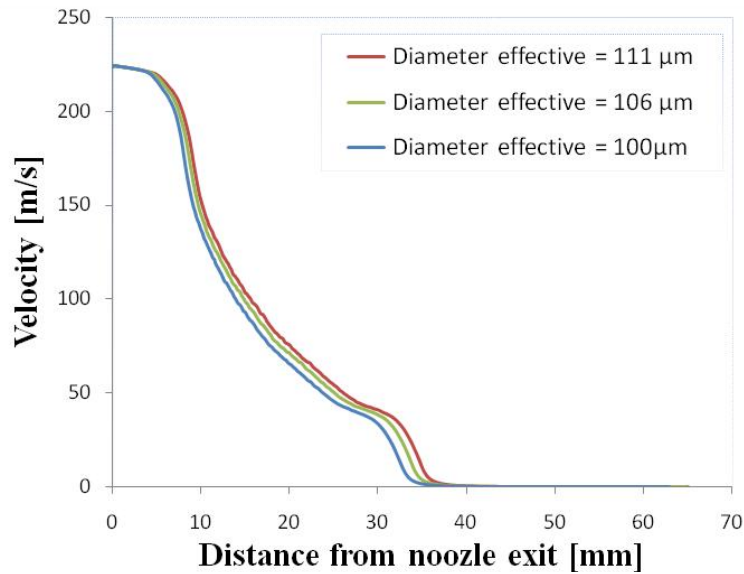


Figure 9: The effect of different effective diameter at 100 $\mu\text{m}$ , 106  $\mu\text{m}$ , and 111 $\mu\text{m}$  on the velocity along the axial axis at the gas ambient temperature of 255 K.

Similarly, the velocity profiles along the axis for three different effective diameters are plotted in Figure 9. As shown in the plot, the velocity at the nozzle exit is identical for three cases, then taking into account the effect of nozzle diameter, the velocity is higher for the larger effective diameter and smaller for the lower effective diameter. All in all, it produced the similar trend. It also proved that the simulation and ELSA model is stable from the beginning to the end of the computed time. The only effect is on the change of particular setup or parameter.

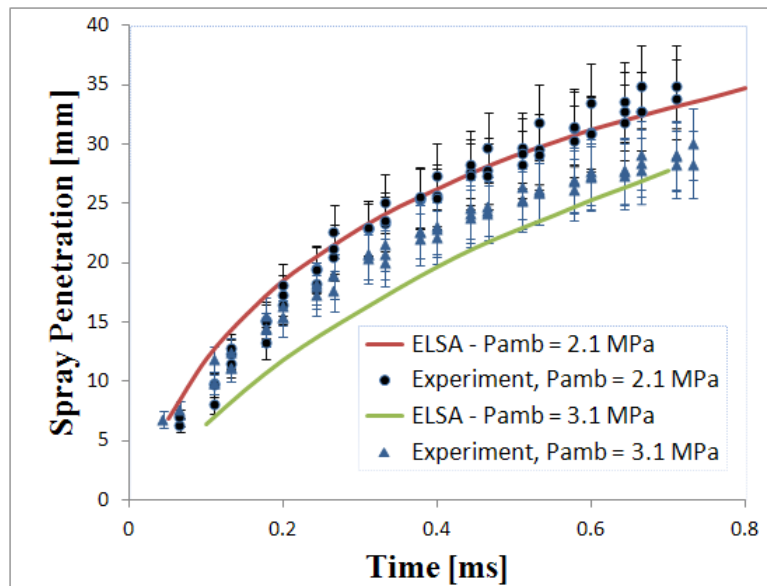


Figure 10: The comparison of spray tip penetration between different ambient pressure 2.1 MPa and 3.1 MPa at the gas ambient temperature of 255 K.

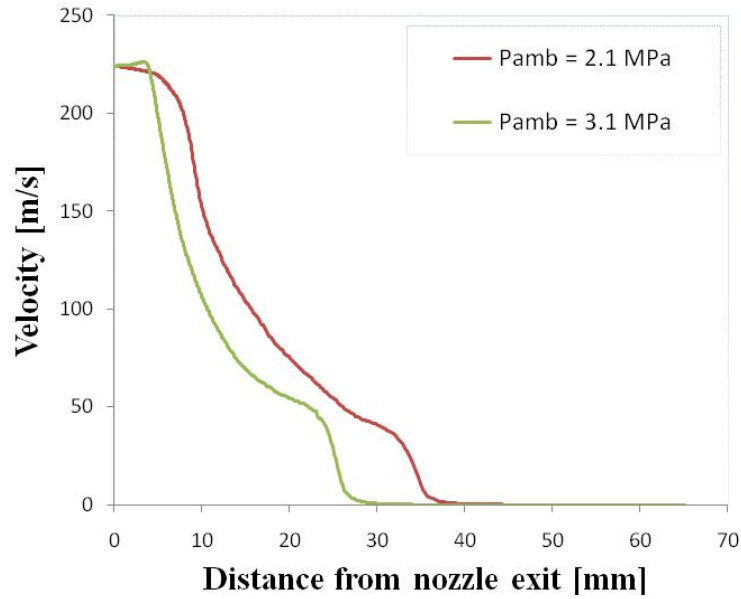


Figure 11: The comparison of velocity profile along the axial axis between different ambient pressure 2.1 MPa and 3.1 MPa at the gas ambient temperature of 255 K.

As shown in Figure 10, the results obtained for both ambient pressure is acceptable in the two computational cases. It is remarkable that the study of spray tip penetration is fitted well with the lower ambient pressure of 2.1 MPa. For the higher ambient pressure of 3.1 MPa, the computational model was illustrated a small difference below 0.4 ms, but still remains within a acceptable range. For the higher computational time after 0.5 ms, the experimental result and simulated case are approached in nearer and nearer. Since the spray penetration mostly concern at the stable value above 0.6 ms, thus the value at 0.7 ms are shown in the plot is very good.

In Figure 11, the assessment of the impact of gas ambient composition variations on the performance of velocity is studied. For the case with ambient pressure of 3.1 MPa, under the higher ambient pressure or in other words, the higher ambient density (as the same temperature and ambient gas are used) the velocity obtained is lower than the case with gas ambient pressure equal to 2.1 MPa.

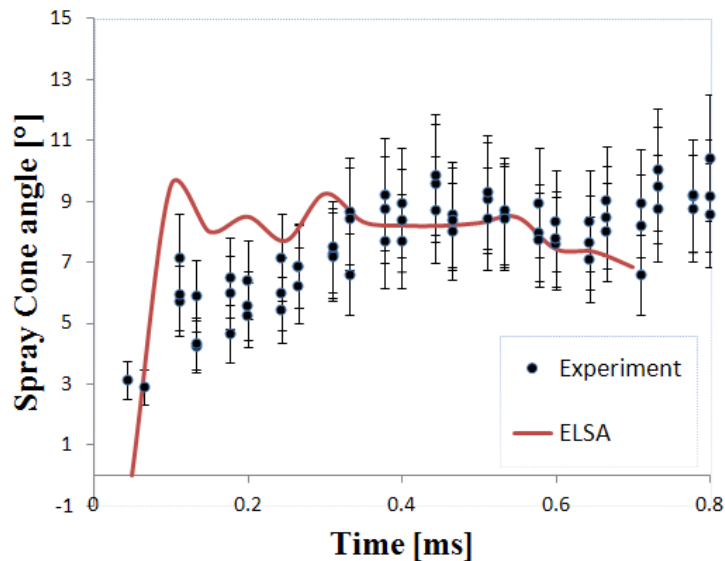


Figure 12: The spray cone angle in the case with  $P_{amb} = 3.1 \text{ MPa}$  ,  $T_{amb} = 255 \text{ K}$ ,  $D_{eff} = 111 \mu\text{m}$ .

Cone angle proposed by Hiroyasu & Arai, 1990 [18] are as following:

$$\theta = 83.5 \left( \frac{1}{d} \right)^{-0.22} \left( \frac{d}{D_o} \right)^{0.15} \left( \frac{\rho_g}{\rho_l} \right)^{0.26} \quad (16)$$

In Figure 12, the spray cone angle depends on time is reported. The simulated results show a close connection with the experimental scatter plot. There is a gap at the beginning of the injection, it happens due to the effect of the fluctuation in mass flow rate and momentum flux measurement from experimental test.

## 6. CONCLUSIONS AND DISCUSSION

Using the same nozzle, injection pressure and injection temperature, the various vessel parameters were investigated in this work. Mostly, we observed the similar results in the comparison with experimental results. All the spray behaviour and its properties are explainable and in line with the theoretical physical approach of the diesel spray in the internal combustion engine.

By using the larger area coefficient, as a linear relation the effective area and effective diameter are increased accordingly. Once we have the higher volume of liquid across the nozzle exit section, the spray tip penetration as well as the velocity tend to have a higher magnitude. For the conical nozzle in which the wide diameter narrow down enough to a smaller outlet diameter, the area coefficient is almost up to 1, and then the cavitation phenomena in the internal nozzle flow is ignored. It is not only occurs in the low temperature, but this is true for any ambient temperature.

The results obtained under the very low temperature aligned well with the experiment result and macroscopic properties of the diesel spray. The change in ambient pressure and ambient density resulted a slightly different in the first few milliseconds at the higher ambient pressure, but it tends to reach experimental data above 0.5 ms.

The article is focused on the assessment of the ELSA model's ability to work in cold starting conditions. With these positive results, the ELSA model can be used to simulate diesel spray in those similar conditions. There is still more investigation to be done and more parameters, temperature should be included to prove its stability and capability to work in all conditions.

## LIST OF ABBREVIATIONS

<b>ARCT</b>	ARCTIQUE
<b>CFD</b>	Computational Fluid Dynamics
<b>DNS</b>	Direct Numerical Simulation
<b>ELSA</b>	Eulerian-Lagrangian Spray Atomization
<b>ITN</b>	Initial Training Network
<b>LES</b>	Large Eddy Simulation
<b>REF</b>	ELITE – Repsol
<b>VECOM</b>	Vehicle Concept Modelling
<b>amb</b>	Ambient
<b>inj</b>	Injection
<b>eff</b>	Effective
<b>g</b>	Gas
<b>l</b>	Liquid

## ACKNOWLEDGEMENTS

This work was supported in part by the Spanish Government in the frame of the Project ‘Métodos LES para la simulación de chorros multifásicos’, Ref. ENE2010-18542 and by Renault. Dung Khuong-Anh has been supported in part by the VECOM (Vehicle Concept Modelling), EU FP7 Marie Curie Initial Training Network (ITN) Grant Agreement 213543 and in conjunction with Renault SA., France.

## REFERENCES

- [1] Vallet A, Burluka AA and Borghi R. Development of a Eulerian model for the atomization of a liquid jet. *Atomization and sprays 2001*; vol. 11, pp. 619-642.
- [2] Blokkeel G, Barbeau B and Borghi R. A 3D Eulerian model to improve the primary breakup of atomizing jet. *SAE Technical Paper 2003*; 2003-01-0005.
- [3] Beau P.A.. Modelisation de l’atomisation d’un jet liquide – Application aux sprays diesel. Ph.D. Thesis, *University of Rouen 2006*.
- [4] Hoyas, S., Pastor, J. M., Khuong-Anh, D., Mompó-Laborda, J. M., Ravet, F.. Evaluation of the Eulerian-Lagrangian Spray Atomization (ELSA) in spray simulations. *International Journal of Vehicle Systems Modelling and Testing 2011*; Vol. 6, Nos. 3/4, pp. 187-201.
- [5] Hoyas, S., Pastor, J. M., Khuong-Anh, D., Mompó-Laborda, J. M., Ravet, F.. Application and evaluation of the Eulerian-Lagrangian Spray Atomization (ELSA) model on CFD Diesel spray simulations. *SAE Paper 2011*; 2011-37-0029.
- [6] Hoyas, S., Gil, A., Margot, X., Khuong-Anh, D., Ravet, F.. Evaluation of the Eulerian-Lagrangian Spray Atomization (ELSA) in spray simulation: 2D cases. *Mathematical and Computer Modelling 2011*; In Press.
- [7] Beau PA (2006). Modelisation de l’atomisation d’un jet liquide – Application aux sprays diesel. Ph.D. Thesis, University of Rouen.
- [8] Ning W, Reitz RD, Lippert AM and Diwakar R.. Development of a next generation spray and atomization model using an Eulerian-Lagrangian methodology. 17th Int. Multidimensional Engine Modeling User’s Group Meeting, Detroit, MI, 2007.
- [9] Desportes, A., Zellat, M., , G.D., D.Abouri, Liang, Y. Validation and Application of the Eulerian-Lagrangian spray atomization. (ELSA) model for the Diesel injection simulation. *SAE Technical Paper*, 2010.
- [10] Desportes, A., Zellat, M., Desoutter, G., Liang, Y., Ravet, F. Application of the Eulerian-Lagrangian spray atomization. (ELSA) model for the Diesel injection simulation. *Conference on Thermo- and Fluid Dynamic Processes in Diesel Engines*, 2010.
- [11] León, G. B.. Experimental and theoretical study of the direct diesel injection process at low temperatures, PhD Thesis. *Universidad Politécnica De Valencia*, 2011.
- [12] Macian, V., Bermudez, V., Payri, R., Gimeno, J. New technique for determination of internal geometry of a diesel nozzle with the use of silicone methodology. *Experimental Techniques*, Blackwell Publishing Ltd, **2003**, Vol. 27(2), pp. 39-43.
- [13] Wilhelm Bosch. The fuel rate indicator: a new measuring instrument for display of the characteristics of individual injection. *SAE Paper 660749*, 1966.
- [14] Allievi, L. . Teoria generale del moto perturbato dell’acqua nei tubi in pressione (colpo d’ariete). (General theory of the variable motion of water in pressure conduits.) *Annali della Società degli Ingegneri ed Architetti Italiani* 17(5), 285-325, Milan, Italy (in Italian), 1902.
- [15] Allievi, L. . Teoria del colpo d’ariete. (Theory of water-hammer.) Nota I-V, *Atti dell’Associazione Elettrotecnica Italiana* 17, 127-150, 861-900 + plates, 1129-1145 + plates, 1235-1253 + plates, and Supplement No 1, 1-35 + plates (in Italian), 1913.

- [16] E. Buckingham. Model experiments and the forms of empirical equations, *Trans Am Soc Mech Eng 1915*; 37,pp. 263–296, 1915.
- [17] J.M. Desantes, R. Payri, J.M. Garcia and F.J. Salvador. A contribution to the understanding of isothermal diesel spray dynamics. *Fuel 2007*; vol. 86, pp. 1093-1101.
- [18] Hiroyasu H. and Arai M.. Structure of fuel sprays in diesel engines. *SAE paper 900475,1990*.